Hindawi Publishing Corporation
Journal of Composites
Volume 2013, Article ID 462914, 11 pages
http://dx.doi.org/10.1155/2013/462914

Research Article

Influence of SiC/Si_3N_4 Hybrid Nanoparticles on Polymer Tensile Properties

Vijaya K. Rangari, M. Yousuf, and Shaik Jeelani

Department of Materials Science and Engineering, Tuskegee University, Tuskegee, AL 36088, USA

Correspondence should be addressed to Vijaya K. Rangari; rangariv@mytu.tuskegee.edu

Received 3 February 2013; Accepted 6 September 2013

Academic Editor: Zhiping Luo

Nanostructured silicon carbide (SiC)/silicon nitride (Si_3N_4) hybrid nanoparticles exhibit a high-potential for reinforcement of polymers. In the present investigation, silicon carbide (β-SiC) nanoparticles (~30 nm) were sonochemically coated on acicular silicon nitride (~100 nm × 800 nm) particles to increase the thermal and mechanical properties of Nylon-6 nanocomposite fibers. To produce Nylon-6/(SiC/Si_3N_4) nanocomposite fibers, we have followed a two-step process. In the first step, SiC nanoparticles were coated on Si_3N_4 nanorods using a sonochemical method and Cetyltrimethylammonium Bromide surfactant. In the second step, the SiC coated Si_3N_4 hybrid nanoparticles were blended with Nylon-6 polymer and extruded in the form of nanocomposite polymer fibers. The nanocomposite fibers were uniformly stretched and stabilized using a two-set Godet roll machine. The diameters of the extruded neat Nylon-6 and SiC/Si_3N_4/Nylon-6 nanocomposite fibers were measured using a scanning electron microscope and then tested for their tensile and thermal properties. These results were compared with the neat Nylon-6 polymer fibers. These results clearly indicate that the as-prepared nanocomposite polymer fibers are much higher in tensile strength (242%) and Young's modulus (716%) as compared to the neat polymer fibers.

1. Introduction

It has always been high interest for the researchers to study the changes in various properties of polymers with the addition of reinforcements. Polymers such as Nylon-6, polypropylene, and LDPE when mixed with an appropriate percentage of nanoparticles as filler materials show significant improvements [1–3]. Many studies have been reported on the structural, chemical, and thermal characterization of nylon [4–7]. Among thermoplastic polymers, Nylon polymers are widely used materials due to low material cost, low density (approximately 12.5% the weight of bronze, 14.3% the weight of cast iron, and 50% the weight of aluminum), wide range of available properties, corrosion resistance, compound customization, insulation qualities, and good load bearing capacity [8]. Many attempts have been made to improve the properties of Nylons with the use of rubber, silica, clay, hydroxyapatite carbon nanotubes, and fibers [9–14]. In these studies, the polymers are blended with appropriate proportions of various shapes and sizes of nanoparticles using various processing techniques to improve mechanical and thermal properties. These materials have been successfully employed in defense, aerospace packing, and electronic and automotive industries. Hence, the improvement of their properties such as mechanical, thermal, electrical, and optical has always been a major point of consideration. Silicon nitride is considered to be a promising ceramic because of its exceptional chemical and mechanical properties, especially at high temperature [15]. Nanostructured silicon nitride particles exhibit a high-potential for the reinforcement of polymers. This covalently bonded material in its larger form exhibits high strength and high toughness and has been used in a number of industrial applications, such as engine components, bearings, springs, high temperature automobile components, and cutting tools [16].

Over the years, a significant progress has been made in the dispersion of acicular nanoparticles in polymer matrices by surface modification and other techniques. While the alignment of acicular or rod shape particles in polymeric

fiber and manufacturing advanced macroscopic structures remain a major challenge. Most commonly used techniques for alignment are wet spinning, [17–19] magnetic alignment, [19] electro spinning [15, 20, 21], and melt processing [22–24]. Nylon is one such widely studied polymer which shows good improvements in mechanical properties when rod-shaped and spherical-shaped nanoparticles are aligned in the preferred direction in the polymer matrix. One of the widely used methods for such an alignment is melt extrusion process. To align the nanoparticles while extruding, a number of aspects should be taken into consideration such as the starting materials and chemical compositions, mixing techniques, type of extruder, material loading process, extrusion temperature, material residence time within the extruder, the die and its orifice shape and size, extrusion rate, extrusion direction, surrounding air temperature and its speed, fibers cooling type and process, and finally the filament draw ratio and winding speed. A proper combination of such factors leads to the production of fine fibers; otherwise, it may cause ambiguity. In our previous studies, we have shown an alignment of Si_3N_4 nanorods in the Nylon-6 polymer through the melt extrusion process [24]. Recent developments in synthesis of silicon based nanoparticle have been resulted in different shapes and sizes of silicon nitride nanoparticles. Among other nanoparticles, the spherical and whisker morphologies are studied extensively. Eblagon et al. [25] have developed an industrial woodcutting inserts from Si_3N_4-based ceramic matrix composites (CMC) and compared with tungsten carbide (WC). It was reported that Si_3N_4/30 wt.% SiC gives the best balance between fracture toughness and wear resistance. Wang and Huang [26] reported that the alignment of whisker could improve the sinterability of the SiC (w)/Si_3N_4 composites without lowering the density. It was also reported that the whisker-oriented alignment led to considerable anisotropy of linear shrinkage and sintering rate of SiC (w)/Si_3N_4 compacts during the sintering. In general, a stable and uniform suspension of acicular nanoparticles in the polymer matrix is required to obtain a fine dispersion and proper alignment of hybrid nanoparticles within the fibers, which are instrumental for the enhancement of structural, thermal, and electrical properties of PNC fibers [23, 24]. In the present study, a sonochemical synthesis technique is used to coat SiC nanoparticles on Si_3N_4 nanorods. The sonochemical effects of ultrasound arise from acoustic cavitations involving the formation, growth, and collapse of bubbles in liquid, which generates localized hot spots having a temperature of roughly 5000 K, pressure of about 20 MPa and very high cooling rates of about $10^7\,K\,s^{-1}$ [24, 25]. These extreme conditions can drive chemical reactions such as oxidation, reduction, dissolution, and decomposition. The sonochemical effects on nanoparticles in ethanol have been well studied [27–29].

In the present study, the SiC nanoparticles were coated on Si_3N_4 using ultrasonic irradiation in presence of ethanol. The as-prepared SiC coated Si_3N_4 nanorods were reinforced with Nylon-6 polymer fibers through the melt extrusion process. Thermal, mechanical, and microscopic analyses were carried out and compared with their neat counterparts.

2. Experimental Procedures

2.1. Materials. The Si_3N_4 (100 × 800 nm) nanorods were obtained from Nanostructured & amorphous Materials, Inc. SiC (30 nm) nanoparticles were purchased from MTI corporation. Commercial Grade UBE Nylon P1011F (Nylon-6, commercial name: Polyamide 6) was procured from UBE America. The physical properties of these materials are presented in Table 1. The density of Nylon-6 is 1.09–1.19 g/cm^3 while the melting point is around 115–225°C. The mechanical property data as provided by the supplier are tensile strength 70–80 MPa, tensile elongation at break 100%, and tensile modulus 1–3 GPa.

2.2. Sonochemical Synthesis of SiC/Si_3N_4 Hybrid Nanoparticles. Sonochemical coating of SiC nanoparticles on rod shaped Si_3N_4 was carried out using a high intensity Sonics Vibra Cell ultrasonic liquid processor (Ti-horn, 20 kHz, 100 W/cm^2). A 1 gm of Si_3N_4, 250 mg of SiC nanoparticles, and 250 mg of CTAB (Cetyl Trimethyl Ammonium Bromide) surfactant in a 60 mL ethanol were mixed well and transferred the reaction mixture to a stainless steel ultrasonic cell jacketed with a circulation of thermostated liquid to maintain a constant temperature of 10°C during the ultrasonic reaction. This reaction mixture was irradiated with ultrasonic horn for 3 hrs in an inert atmosphere of nitrogen gas. The resulting reaction mixture is separated from ethanol by using a high speed Allegra 64 R centrifuge at a speed of 10,000 rpm and 10°C. The precipitate was washed at least 5 times with ethanol to remove the CTAB. The resulting hybrid nanoparticles of SiC/Si_3N_4 were kept in a vacuum oven for overnight at room temperature to dry the particles and these particles were used for analysis and reinforcements in Nylon-6 fibers.

2.3. Melt Processing. SiC-coated rod-shaped Si_3N_4 particles and Nylon-6 powder were carefully measured in the ratio of 1 : 99 by weight. The dry mixing of Nylon-6 powder with SiC/Si_3N_4 particles was carried out in a mechanical blender in a circulating cold base container (5°C) at a speed of 2300 rpm. The mixing process was paused for 6 minutes after 3 minutes of continuous mixing and then resumed for further mixing. This was done to avoid temperature rise, which may result in softening the Nylon-6. This technique is repeated 20 to 30 times until uniform mixing was observed. The effective time for which the mixture was blended was between 75 to 90 minutes. At this time the mixture took a light gray appearance and it seemed that the SiC/Si_3N_4 was thoroughly mixed with the Nylon-6. The same process was repeated for rod-Si_3N_4 and SiC nanoparticle mixing with Nylon-6 polymer to ensure proper blending. The reinforcement of higher concentrations of hybrid nanoparticles was not studied because of the problems encountered in extrusion of polymer fibers due to particle agglomeration.

The mixture of Nylon-6 and Si_3N_4 nanoparticles was then further air dried in a dryer for 12 hrs and extruded using a Wayne Yellow Label Table Top single screw extruder. The extruder has a 19 mm diameter screw, which is driven by a 2 HP motor via toothed timing belt for smooth speed reversal

Table 1: As-received material properties.

Type	Morphology	Size	Manufacturer	Density (g/cm^3)	Color
Nylon-6	Irregularly shaped	100–500 μm	UBE America, Inc	1.09–1.19	White
Si_3N_4	Rod-shaped (Alpha, 99%)	100 × 800 nm	Nanostructured and amorphous Materials, Inc	Bulk 0.03–0.05 True 3.44	Light gray
SiC	Spherical	~30 nm	MTI corporation	1.09–1.19	Black

and encased inside the barrel. Thermostatically controlled five heating zones were used to melt the mixture prior to extrusion; three of which were occupied by the barrel zone and the rest of the two were by the die zone. The heaters inside the barrel zone were placed at the feed hopper side, center, and die zone side of the barrel and set at a temperature of 226.67°C, 235°C, and 243.33°C, respectively. The purpose of these three heaters is to maintain gradually increasing temperature in the molten mass. The process begins when the nanophased dry-mixed powder is poured through the feed hopper to get inside the barrel zone of the extruder. As soon as it reaches the barrel zone, Nylon-6 starts melting due to high barrel temperature. At this stage, the whiskers particles are randomly distributed within the liquid matrix. The outer surface of the screw is designed to maintain a close fit with the barrel inner surface. As a result, the molten mass cannot escape from the screw surface and are trapped inside the screw segment. As the extruder screw rotates, this molten matrix is slightly mixed with the nanoparticles, conveyed in a spiral pattern and finally reaches the screw end which is located immediately before the die zone. The screw end is shaped in such a way that it allows the flowing mass to escape through a narrow opening at high velocity. As the screw rotation is continued, the high velocity liquid experiences an enormous shear force. The shear force at this high temperature can alter the chemical and thermal properties of the nylon 6 and also the orientation of rod-shaped and spherical particles. It is assumed that the rod shape/spherical particles are partially aligned at this stage. The partially aligned rod shape particles containing liquid nylon 6 now enter the die zone which is constructed with a circular plate, 10 cm long steel tubing with 4 mm inner diameter, and the die itself. The two heaters at this zone are set at a temperature of 245°C to maintain constant temperature of the flowing mass. One of the heaters is placed after the circular plate and the other one is placed immediately before the die. The circular plate is 15 mm in diameter and contains about 20 orifices, each of which is 2 mm in diameter. As the bulk materials are passing through the plate, they are disintegrated into several branches, and then combined again. This ensures a distributive mixing of the nanoparticles with Nylon-6. Now partially aligned nanoparticles containing liquid Nylon-6 are passed through the 10 cm long steel tube and arrive close to the die. It should be noted that in order to ensure proper alignment of fiber, the size of the die plate and the diameter of the die opening are very critical. Hence, a special type of die was used in this process, which has a converging inlet and a narrow outlet (1 mm). This die configuration generates two distinct flow regimes that highly affect the fiber alignments. First, the converging die inlet introduces a converging flow pattern, which in turn aligns the fibers along the stream line direction. Second, the narrow orifice allows the flow pattern to transform into shear flow as it enters the narrow orifice. The shear flow produces additional fiber alignment due to differential shear rate along the boundary layer that orients the fibers in the direction of the flow.

The process is continuous and the composite fibers with constant tension were extruded at a screw speed of 8–10 rpm and feed rate of approximately 80 g/h. Fibers were allowed to travel from the water bath, the water at room temperature of 20°C to a set of tension rollers, winder guide rollers, then wound on a spool using Wayne Desktop Filament Winder at a winding speed of 45 rpm. The process temperature, speed ratio between the winder and extruder screw, the position of the roller guide, and filament travel distance, all these factors control the draw ratio of the process as well as the continuity of the fibers.

2.4. Characterization. The X-ray diffraction (XRD) measurements were carried out using a Rigaku D/MAX 2200, X-ray diffractometer with Cu Kα radiation at 40 kV and 30 mA. The (2θ) angles of diffraction were measured from 10 to 80° in the equatorial direction to understand the crystalline nature of as-received nanoparticles and its hybrid nanoparticles. These samples were prepared by spreading uniformly powder nanoparticles on to a quartz glass sample holder and XRD tests were conducted. Differential scanning calorimetry (DSC) experiments were carried to measure the glass transition temperatures, heat of enthalpy, and melting points of neat Nylon-6 and nanoparticles reinforced Nylon-6 nanocomposite fibers. These experiments were carried out using a Mettler Toledo DSC 822^e from 30°C to 300°C at a heating rate of 5°C/min under nitrogen atmosphere.

The as-received and as-prepared nanoparticles shapes and sizes were characterized using JEOL-2010 transmission electron microscope (TEM) and scanning electron microscope (JEOL-5800). The TEM samples were prepared by dropping a colloidal solution of nanopowder in ethanol on to a carbon-coated copper grid, whereas SEM samples were prepared by placing a powder sample on double-sided carbon tape and coated with gold palladium to avoid the sample charging. Single fiber tensile tests were conducted on Zwick-Roell tensile testing equipment with a 20 N load cell. These tests were carried out under displacement control at a crosshead speed of 0.011/s strain rate and gage length of 102 mm (ASTM standard D 3379-75) [30].

3. Results and Discussion

The as-received and hybrid nanoparticles were analyzed using X-ray diffractometer. The technique was used to study the crystallinity and coating of SiC nanoparticles on Si_3N_4 nanorods. X-ray diffraction patterns reveal that the as-received SiC, Si_3N_4, and synthesized SiC/Si_3N_4 nanoparticles are highly crystalline. Figure 1 depicts the powder XRD patterns of (a) as-received SiC, (b) as-received Si_3N_4, and (c) SiC coated Si_3N_4. Figure 1(a) shows the XRD peaks of SiC nanoparticles (b) Si_3N_4 nanorod particles and match very well with JCPDF no. 29–1129 and JCPDF no. 41–0360 respectively. Figure 1(c) shows the XRD peaks of SiC coated Si_3N_4 hybrid nanoparticles and all the peaks are assigned to SiC and Si_3N_4 particles. The 100% peak of SiC nanoparticles is submerged in Si_3N_4 peak and we can clearly see the peak widening ~35 of two theta degrees of SiC/Si_3N_4 hybrid nanoparticles. It should be noted that the peak intensities of Si_3N_4 are also decreasing after coating with SiC nanoparticles on Si_3N_4. These results indicate that the SiC nanoparticles are coated on Si_3N_4. Similar results were also observed by other researchers [31].

SEM analysis was carried out to study the shape and sizes of as-received Nylon-6 polymer powder and presented in Figure 2(a). The micrograph shows that the Nylon-6 polymer powder is irregular in shape and ~100 to 500 μm in sizes. TEM analysis was also carried out to study the shape and sizes of as-received SiC, Si_3N_4, and extent of SiC coating on Si_3N_4 nanorods. Figures 2(b) and 2(c) show the TEM picture of the as-received spherical SiC and Si_3N_4 nanorods. The sizes measured from the micrographs are ~30 nm in diameter for SiC and 100–500/80 nm in length/width for Si_3N_4. Figure 2(d) depicts the SiC coated Si_3N_4 nanorods. This micrograph clearly shows that the SiC nanoparticles are evenly coated on Si_3N_4 nanorods and the particle sizes of SiC and Si_3N_4 marches very well with the as-received materials. Figure 2(e) represents a high resolution micrograph of one of the SiC nanoparticles coated Si_3N_4 nanorod. This micrograph also shows the lattice spacing of (111) and (100) planes of SiC and Si_3N_4, respectively. The crystal average d-spacing of 0.25 nm and 0.68 nm confirms the presence of both SiC and Si_3N_4 together.

SEM analysis was also carried out for as-extruded single fibers to study the smoothness of the fibers and measure the accurate dimensions to use in tensile strength calculations. The SEM images in Figures 3(a), 3(b), 3(c), and 3(d) show the surfaces and diameters of continues single fibers of (a) Neat Nylon-6, (b) SiC/Nylon-6, (c) Si_3N_4/Nylon-6, and (d) SiC-coated Si_3N_4/Nylon-6 polymer fibers. The surfaces of these fibers are almost smooth and uniform, no physical defects were observed along the length of the fiber. The diameters measured for these single fibers are ~100 μm, 85 μm, 80 μm, and 75 μm, respectively for (a) Neat Nylon-6, (b) SiC/Nylon-6, (c) Si_3N_4/Nylon-6, and (d) SiC-coated Si_3N_4/Nylon-6. These diameters were used in calculating the tensile strength and modulus of the single fibers. Figures 4 and 5 display the DSC curves obtained from heating and cooling of (a) Neat Nylon-6, (b) Si_3N_4/Nylon-6, (c) SiC/Nylon-6, and (d) SiC-coated Si_3N_4/Nylon-6 filaments obtained from the extrusion

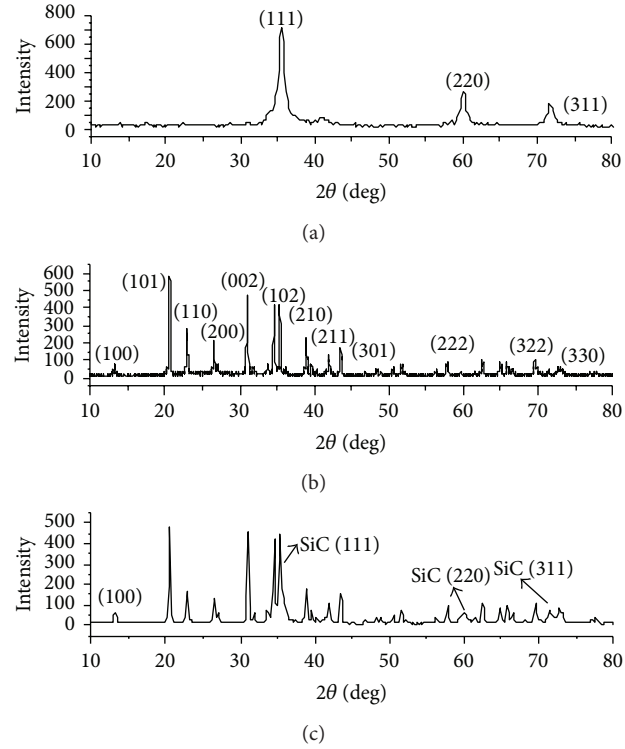

Figure 1: XRD patterns of (a) as-received SiC, (b) as-received Si_3N_4, and (c) SiC coated Si_3N_4.

process. These results are also presented in Table 2. In this study, the *Tgs* were measured as the inflection points of the heat flow curves [32, 33]. Table 2 clearly shows that the *Tgs* of extruded Nylon-6 has increased from 80°C to 130°C maximum with the reinforcement of 1 wt% rod Si_3N_4 nanoparticles. We have also observed the increase in Tg for the reinforcement of SiC and SiC coated Si_3N_4 nanoparticles from 80°C to 94°C and 126°C, respectively. This increase in *Tg* is due to the presence of Si_3N_4, SiC, and their SiC/Si_3N_4 hybrid nanoparticles, which may have imposed restrictions in molecular mobility at earlier stages. This effect can also be understood in terms of decreasing free volume of the polymer. From the concept of free volume, it is known that, in the liquid state when free space is high, molecular motion is relatively easy because of the unoccupied volume. As the temperature of the melt is lowered, the free volume would be reduced until there would not be enough free space to allow molecular motion or translation. With the reinforcement of Si_3N_4, SiC and SiC-coated Si_3N_4 nanoparticles, this free space is evidently further reduced [34, 35]. The melting temperature *Tm* of polymers that can crystallize such as Nylon-6 has been linked with their chemical structure. Three factors influence this link: chain geometry and regularity, chain stiffness, and hydrogen bonding within nylon [36]. It has been reported in the literature that the nanoparticles can act as sites of nucleation sites for polymer crystals [37, 38]. According to Table 2, there is a considerable difference in the melting temperatures of the neat Nylon-6 and Si_3N_4, SiC and SiC-coated Si_3N_4 reinforced Nylon-6. This is confirmed by

Table 2: DSC results of neat and nanoparticles infused Nylon-6 nanocomposite fibers.

Sample	Tg (°C)	Tm (°C)	Tr (°C)	ΔH_m (J/g)	% Crystallinity	% Increase
Neat Nylon-6 fiber	80	225.5	187.4	61.8	106.6	6.6
Nylon-6/1 wt% rod-Si_3N_4	130	226.2	191.8	99.1	170.9	64.2
Nylon-6/1 wt% SiC	94	229.2	193.5	103.5	178.4	71.7
Nylon-6/1 wt% SiC-coated rod-Si_3N_4	126	229.2	194.3	103.3	178.1	71.4

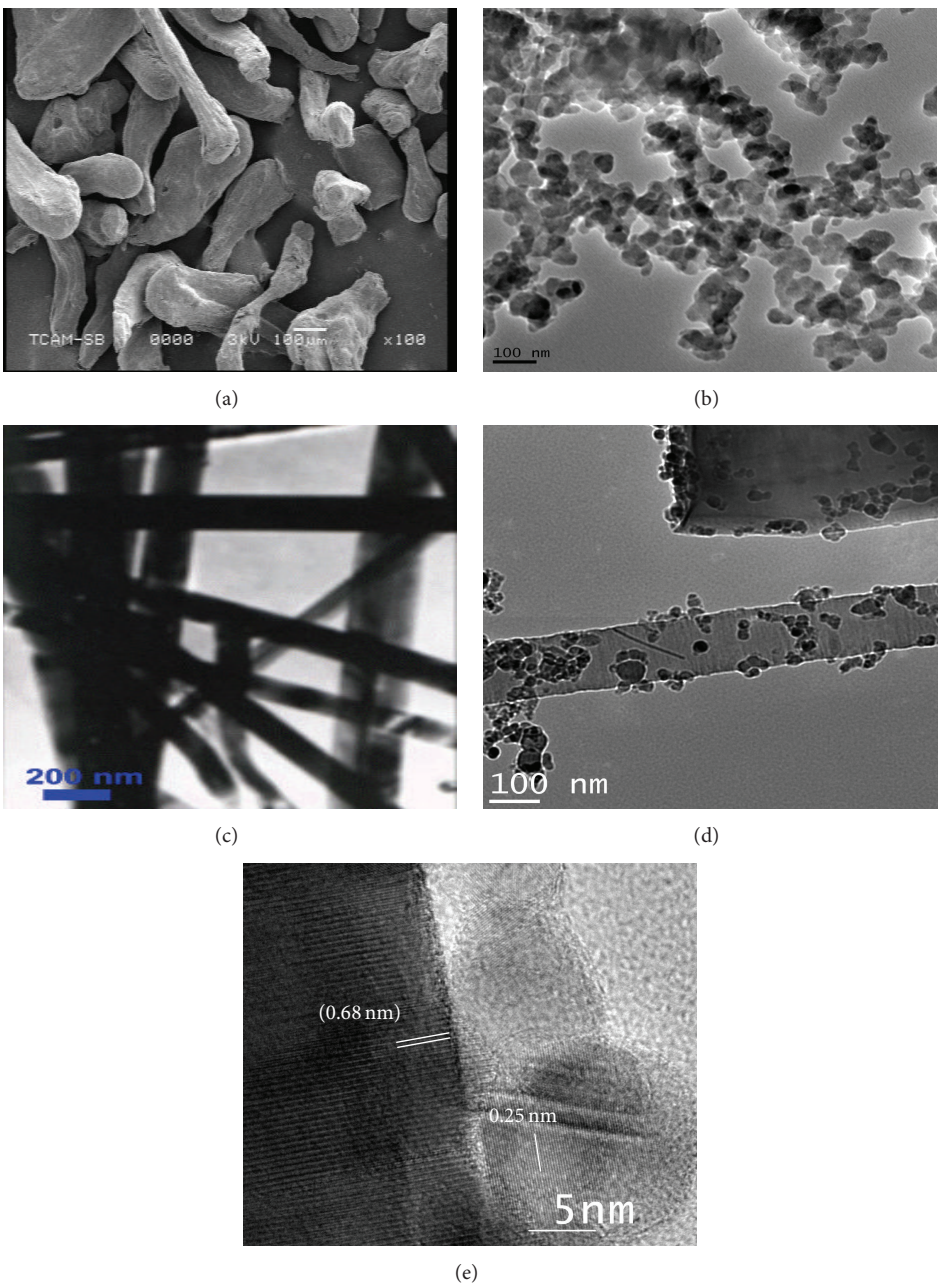

Figure 2: SEM micrograph of as-received (a) Nylon-6 polymer powder, TEM micrograph of as-received, (b) SiC, (c) Si_3N_4 and (d) SiC coated Si_3N_4, (e) high-resolution micrograph of SiC nanoparticle coated Si_3N_4 nanorod.

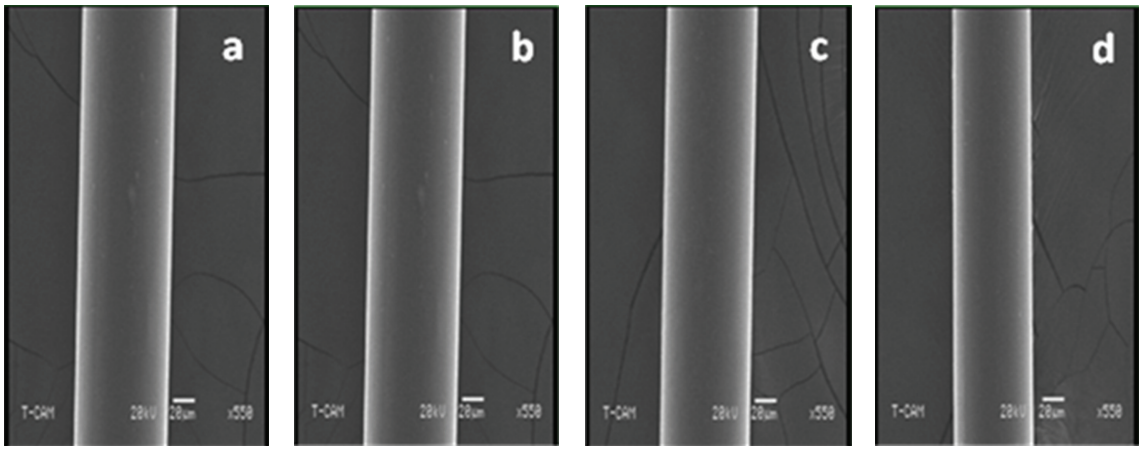

Figure 3: SEM micrograph of as-extruded (a) Neat Nylon-6, (b) SiC/Nylon-6, (c) Si_3N_4/Nylon-6, and (d) SiC coated Si_3N_4/Nylon-6 polymer fibers.

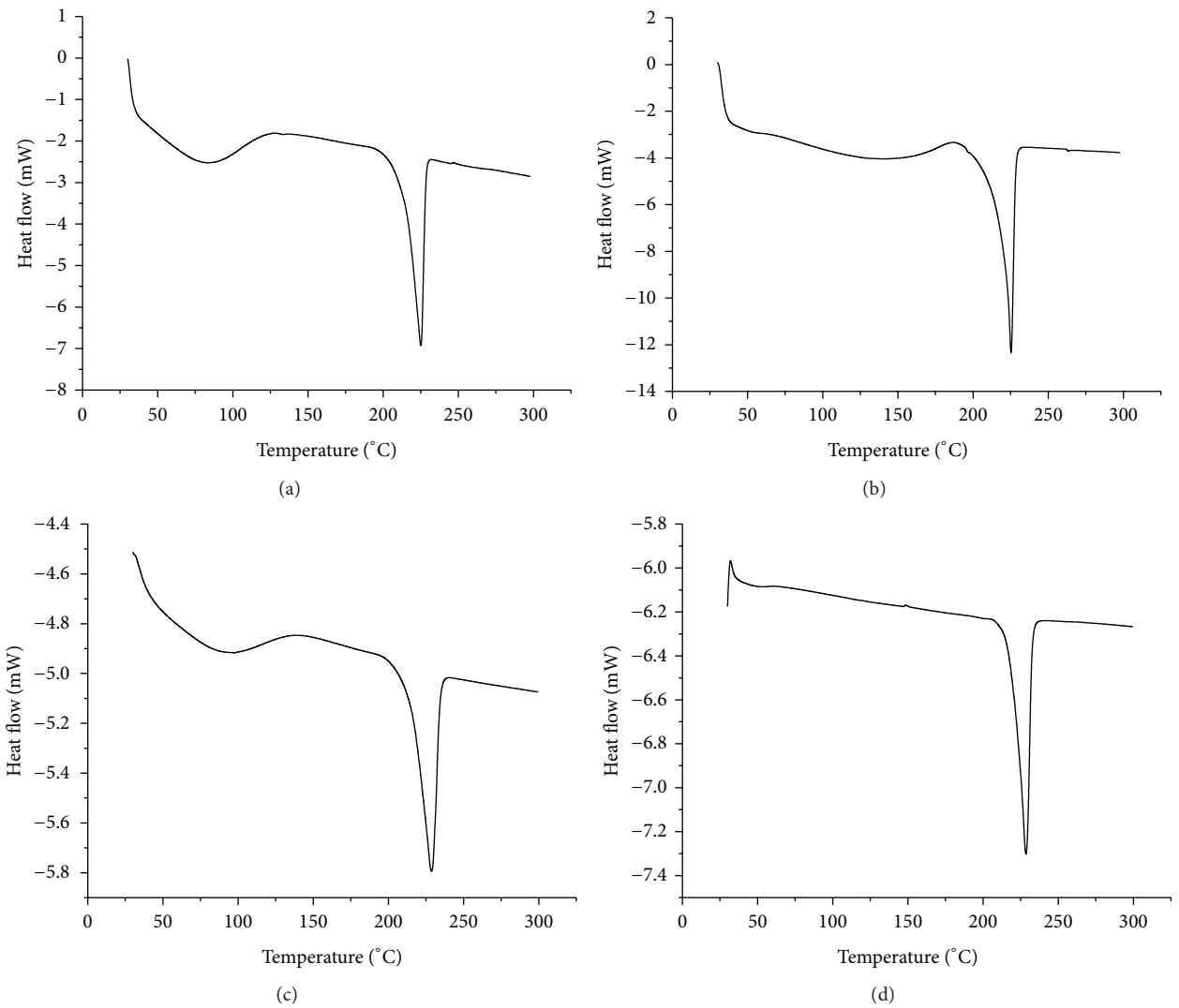

Figure 4: DSC melting curves of (a) Neat Nylon-6, (b) Si_3N_4/Nylon-6, (c) SiC/Nylon-6, and (d) SiC coated Si_3N_4/Nylon-6 filaments.

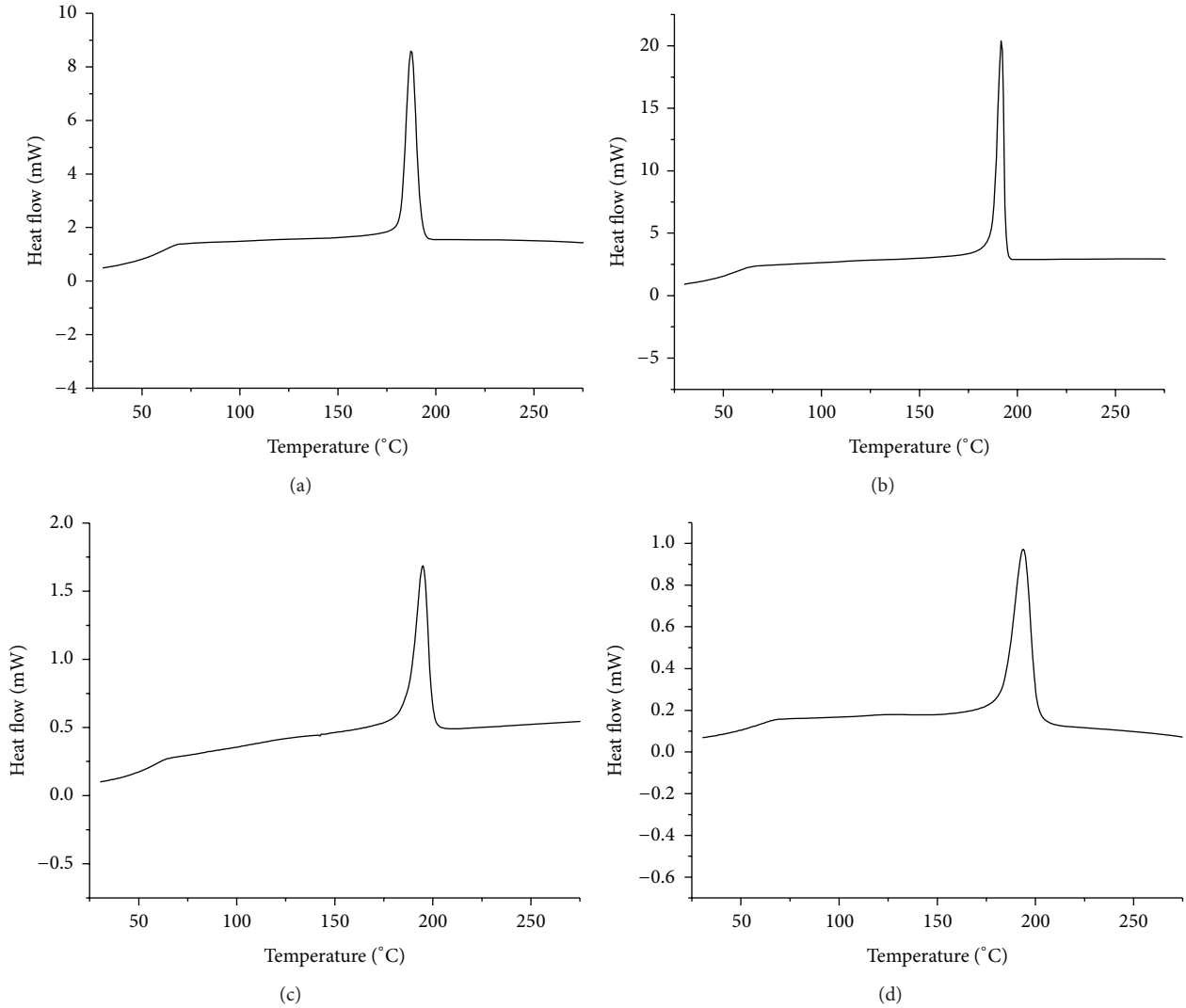

Figure 5: DSC cooling curves of (a) Neat Nylon-6, (b) Si_3N_4/Nylon-6, (c) SiC/Nylon-6, and (d) SiC coated Si_3N_4/Nylon-6 filaments.

the variation of crystallinity of the neat and the degrees of crystallinity, calculated from melting endotherm (Figure 4) and heats of fusion, which are 6.7%, 64.26%, 71.79%, and 71.45%, respectively, for neat Nylon-6, Si_3N_4, SiC, and SiC-coated Si_3N_4 reinforced Nylon-6 nanocomposite fibers, respectively. Similar results were observed in our earlier studies as well [25]. These results are also consistent with X-Ray studies.

3.1. Tensile Response. Tensile tests of single-fiber specimens of the neat Nylon-6 and composites infused with, Si_3N_4, SiC, and SiC-coated Si_3N_4 fibers were carried out to estimate the increase in tensile properties, such as strength and modulus. The tests were performed according to the ASTM standard D 3379-75 [30]. The results of tensile properties of the (a) neat Nylon-6, (b) 1.0 wt% Si_3N_4/Nylon-6, (c) 1.0 wt% SiC/Nylon-6, and (d) 1.0 wt% SiC-coated Si_3N_4/Nylon-6 fibers are shown in Figure 6 and summarized in Table 3. The ultimate tensile strength values for neat Nylon-6, 1.0 wt%, Si_3N_4/Nylon-6, SiC/Nylon-6, and SiC-coated Si_3N_4/Nylon-6 fibers are 248 Mpa, 687 MPa, 371 MPa, and 602, respectively. The modulus is also significantly increased ~716% as compared to the neat Nylon-6.

The SiC-coated Si_3N_4 hybrid nanoparticles infused Nylon-6 exhibit a greater stiffness and higher value of Young's modulus when compared to the individual SiC and Si_3N_4 reinforcements. The main reason may be that the SiC nanoparticles are uniformly adhered to the surface of the Si_3N_4 rods and they provide better interaction with the polymer matrix. The interfacial bonding and the cross liking with the polymer is better exhibited by such coated Si_3N_4 particles. The effect is as if it is the combine synergistic effect of the SiC particles and the Si_3N_4 particles together. This clearly suggests that the sonochemical coating of SiC on Si_3N_4 better hybridization which improves the better alignment as well as better adhesion to the polymer matrix.

As we derive the results from the tensile testing of single filaments of Nylon-6 and the Nylon-6 filaments reinforced with the various fillers, it becomes important that we study and explain the characteristics of the curves obtained.

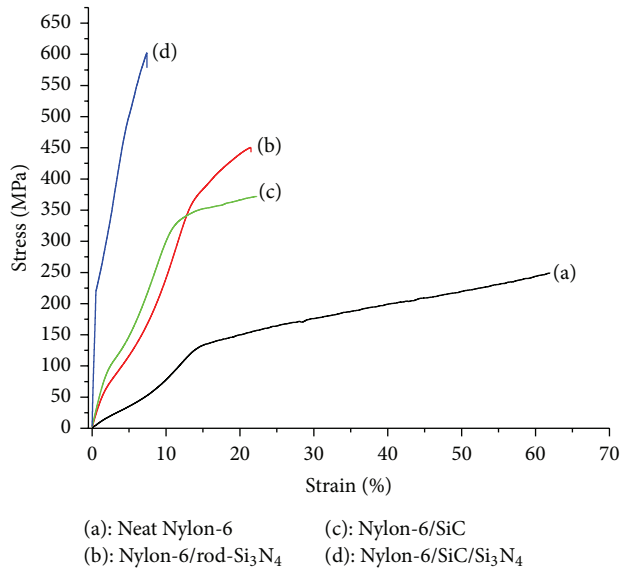

Figure 6: Tensile response of (a) Neat Nylon-6, (b) Si_3N_4/Nylon-6, (c) SiC/Nylon-6, and (d) SiC coated Si_3N_4/Nylon-6 filaments.

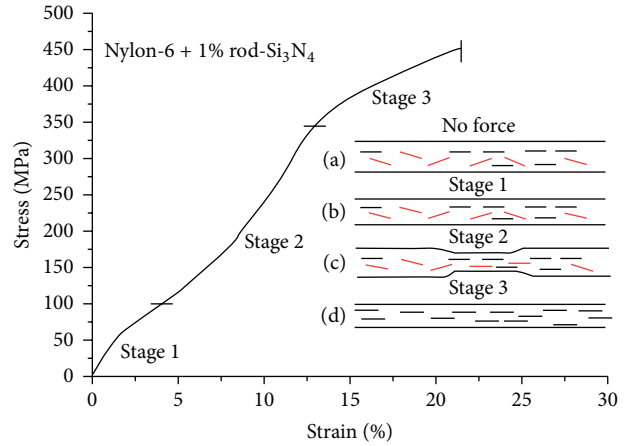

Figure 7: Tensile stress-strain curves a fiber at various stages (a) fiber before subjected to the tensile force, (b) Fiber initial stretching the stage 1, (c) fiber necking the stage 2, of (d) complete stretching and stage 3, complete stretching of the filament length, and diameter reduction.

The response of the nylon filaments to the application of the tensile force is recorded in a particular pattern curve. The following is an explanation of what physically happens to the filament during the test. This is clearly explained in the Figure 7 with various stages of particles alignment in the single fiber.

As shown in Figure 7(a), the fiber is in its original diameter and length before being subjected to the tensile force. Although the single screw extrusion process aligns the rod-Si_3N_4 in the Nylon-6 fiber [24] while stretching and there are some unaligned rod-Si_3N_4 left in the Nylon-6 fiber. When the force is applied to the ends of the fiber (tensile testing), the initial stretching of the fiber starts and is shown as the stage 1 of the fiber stretching in the Figure 7(a). At this

Table 3: Tensile properties of neat and nanoparticles infused Nylon-6 nanocomposite fibers.

Type	Strength, (MPa)	% Increase in strength	Modulus (MPa)	% Increase in modulus
Neat Nylon-6	248	—	0.55	—
Nylon + 1 wt% Si_3N_4	450	181	3.36	510.9
Nylon + 1 wt% SiC	371	149	3.28	496.36
Nylon + 1 wt% Si_3N_4/SiC	602	242	4.49	716.36

initial stage, the tensile response is a linear curve from the origin and is generally used to calculate the modulus. The fiber experiences reduction in its diameter and increases in length until the necking of the fiber starts. The necking of the fiber continues as shown in Figure 7 as stage 2 of the fiber stretching. The diameter of the fiber gets smaller at the necking region. Due to this event, the rod shaped particles (Si_3N_4) are forced to straighten and consequently get aligned in the axial direction. This phenomenon is represented in Figure 7(b). Such reduction of diameter occurs until the complete length of the fiber gets to this uniform diameter. The dip in the curve obtained due to the tensile testing is assigned to stage 2. We predict that all the unaligned rod-shaped particles get aligned throughout the length of the fiber at stage 2 and the fiber shows a higher strength than in stage 1. The final stage, stage 3, as shown in Figure 7 is the fiber resistance to the applied force to it to a higher extent and the dip in the tensile testing curve starts to form linear. An interesting situation to know here is that after stage 2, the Nylon-6 polymer chains are also stretched along with the rod-shaped particles in the direction of loading and entangled polymer chains to resist the tensile force until breakage point. This is the point where the complete failure occurs and measured as ultimate tensile strength. The extent of this failure depends on the polymer used and the percentage loading and aspect ratio of nanoparticles. A perfect combination of these will give strengths which possibly cannot be acquired through the neat polymers without fillers. The above graph (Figure 6) represents the curve obtained when Nylon-6/rod shaped silicon nitride fibers are subjected to tensile test. The three stages of stretching and the failure can be seen in the graph. The stages 1, 2, and 3 occur in the neat systems also, except that the neat systems do not have anything to resist the tensile forces except for their polymer chains. Hence, we can observe that the neat systems dip in the curve and slope of the linearity are far lesser than those of their composite fibers. Interestingly we can also see that the stress-strain curve for SiC/Si_3N_4 Nylon-6 polymer composite fibers in stage 2 is almost insignificant. The reason for this may be the strong interaction between SiC/Si_3N_4 hybrid nanoparticles with Nylon-6 polymer chains where there is highly restricted polymer chain motion.

To understand further details of the tensile test results, we have carried out the SEM analyses of tensile failure fracture surface of (a) Neat Nylon-6, (b) Si_3N_4/Nylon-6, (c) SiC/Nylon-6, and (d) SiC-coated Si_3N_4/Nylon-6 fibers are

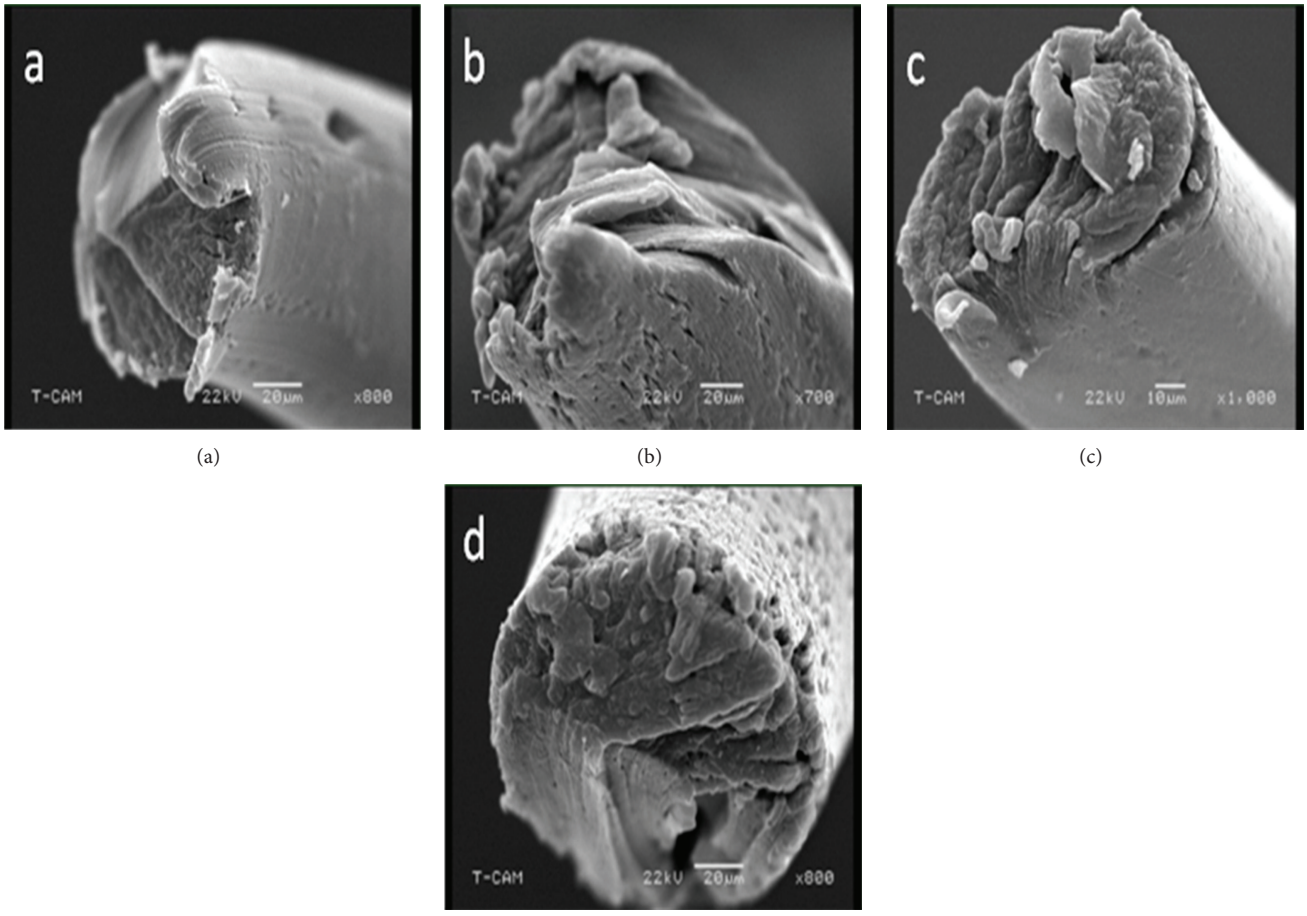

(a) (b) (c)

(d)

Figure 8: SEM micrograph of fracture surface of (a) Neat Nylon-6, (b) Si_3N_4/Nylon-6, (c) SiC/Nylon-6, and (d) SiC coated Si_3N_4/Nylon-6 filaments.

shown in Figure 8. This Figure shows that the cross-sectional area of the fibers was circular and the failure was initiated at the edge of the fiber. Since the size of rod Si_3N_4 and SiC particles are very small, ranging from 20 to 30 nm in diameter, the pores within the structure could be an indication of nanoparticles integrated within the Nylon-6 composite fiber matrix which detached during fracture, described as particle matrix de-bonding during deformation [39]. The even distribution of pores throughout the cross-section could imply that the nanoparticles domains were evenly distributed through the fracture surface. It is also seen in the micrograph that many craze normal to the tensile direction are found at the side surface of specimen Figures 8(a)–8(d). Craze grows bigger and joins together to form cracks. For neat Nylon-6, craze is minimum compared to the nanoparticles infused Nylon-6 fiber. Maximum craze can be seen for Nylon-6 with SiC/Si_3N_4 hybrid nanoparticles indicating stronger resistance to crack propagation. In general, the fibers stress at fracture is also the ultimate stress. Upon reaching the point of ultimate stress, there was no sign of any further elongation before fracture. This could be attributed to the small dimensions of the fibers that caused instability during the initial stage of neck formation and, hence, fracture to take place easily as in the case of neat Nylon-6.

4. Conclusions

SiC/Si_3N_4 hybrid nanoparticles were synthesized using the sonochemical method. Neat Nylon-6, SiC, Si_3N_4, and SiC/Si_3N_4 infused Nylon-6 polymer composite fibers were fabricated using a single screw melt extruder. XRD and TEM studies reveal that SiC nanoparticles were uniformly coated on Si_3N_4 surfaces. The improvement in ultimate tensile strength and elastic modulus is attributed to the alignment of the SiC/Si_3N_4 nanoparticles along the extrusion direction. The increase in thermal stability and crystallinity of SiC/Si_3N_4-infused Nylon-6 PNC is correlated with the better cross-linking between the nanoparticles and the polymer matrix. The in situ 1% SiC/Si_3N_4 Nylon-6 nanocomposite fibers were demonstrated to have an excellent strength when compared to the neat Nylon-6. It is also noteworthy to mention that this sonochemical synthesis technique can be used to synthesize SiC/Si_3N_4 hybrid nanoparticles in bulk quantities. Overall, this technique can be adapted

for fabrication of other multifunctional nanomaterials for specific application.

Conflict of Interests

The authors declare that there is no conflict of interests in this paper.

Acknowledgments

The authors would like to thank the National Science Foundation for their financial support through NSF-NSF-RISE #113768 and AL-EPSCoR #1158862 and also the UBE Corporation for providing Nylon-6 polymer for this research.

References

[1] J. Jin, R. Rafiq, Y. Q. Gill, and M. Song, "Preparation and characterization of high performance of graphene/nylon nanocomposites," *European Polymer Journal*, vol. 49, no. 9, pp. 2617–2626, 2013.

[2] Y. Lin, H. Chen, C.-M. Chan, and J. Wu, "Effects of coating amount and particle concentration on the impact toughness of polypropylene/$CaCO_3$ nanocomposites," *European Polymer Journal*, vol. 47, no. 3, pp. 294–304, 2011.

[3] K. Sarita, K. Susheel, C. Annamaria, N. James, H. Youssef, and K. Rajesh, "Surface modification of inorganic nanoparticles for development of organic-inorganic nanocomposites: a review," *Progress in Polymer Science*, vol. 38, no. 8, pp. 1232–1261, 2013.

[4] P. S. Song, S. Hwang, and B. C. Sheu, "Strength properties of nylon- and polypropylene-fiber-reinforced concretes," *Cement and Concrete Research*, vol. 35, no. 8, pp. 1546–1550, 2005.

[5] Y. Li, Z. Huang, and L. Yandong, "Electrospinning of nylon-6,66,1010 terpolymer," *European Polymer Journal*, vol. 42, no. 7, pp. 1696–1704, 2006.

[6] N. Noda, Y.-H. Lee, A. J. Bur et al., "Dielectric properties of nylon 6/clay nanocomposites from on-line process monitoring and off-line measurements," *Polymer*, vol. 46, no. 18, pp. 7201–7217, 2005.

[7] V. K. Rangari, M. M. Ghouse, S. Boyoglu, and S. Jeelani, "Synthesis of hybrid ZnO/CNTs nanoparticles and their reinforcement in Nylon-6 polymer fibers," *Journal of Applied Polymer Science*, vol. 129, pp. 121–129, 2013.

[8] A. S. Khan and B. Farrokh, "Thermo-mechanical response of nylon 101 under uniaxial and multi-axial loadings: part I, experimental results over wide ranges of temperatures and strain rates," *International Journal of Plasticity*, vol. 22, no. 8, pp. 1506–1529, 2006.

[9] G. Monserrat, B. Jonathan, E. Ramon et al., "Hybrid organic inorganic nylon-6/SiO_2 nanocomposites: transport properties," *Polymer Engineering and Science*, vol. 44, no. 7, pp. 1240–1246, 2004.

[10] R. Scaffaro, L. Botta, A. Frache, and F. Bellucci, "Thermo-oxidative ageing of an organo-modified clay and effects on the properties of PA6 based nanocomposites," *Thermochimica Acta*, vol. 552, no. 20, pp. 37–45, 2013.

[11] D. Weifu, L. Yiqun, Z. Xiaohong et al., "Preparation of high barrier and exfoliated-type nylon-6/ultrafine full-vulcanized powdered rubber/clay nanocomposites," *Macromolecules*, vol. 38, no. 11, pp. 4551–4553, 2005.

[12] W. D. Zhang, L. Shen, I. Y. Phang, and T. Liu, "Carbon nanotubes reinforced nylon-6 composite prepared by simple melt-compounding," *Macromolecules*, vol. 37, no. 2, pp. 256–259, 2004.

[13] L. Qu, L. M. Veca, Y. Lin et al., "Soluble nylon-functionalized carbon nanotubes from anionic ring-opening polymerization from nanotube surface," *Macromolecules*, vol. 38, no. 24, pp. 10328–10331, 2005.

[14] X. Ji, J. E. Hampsey, Q. Hu, J. He, Z. Yang, and Y. Lu, "Mesoporous silica-reinforced polymer nanocomposites," *Chemistry of Materials*, vol. 15, no. 19, pp. 3656–3662, 2003.

[15] F. Ko, Y. Gogotsi, A. Ali et al., "Electrospinning of continuous carbon nanotube-filled nanofiber yarns," *Advanced Materials*, vol. 15, no. 14, pp. 1161–1165, 2003.

[16] B. Vigolo, A. Penicaud, C. Coulon et al., "Macroscopic fibers and ribbons of oriented carbon nanotubes," *Science*, vol. 290, no. 5495, pp. 1331–1334, 2000.

[17] S. Kumar, T. D. Dang, F. E. Arnold et al., "Synthesis, structure, and properties of PBO/SWNT composites," *Macromolecules*, vol. 35, no. 24, pp. 9039–9043, 2002.

[18] B. Vigolo, P. Poulin, M. Lucas, P. Launois, and P. Bernier, "Improved structure and properties of single-wall carbon nanotube spun fibers," *Applied Physics Letters*, vol. 81, no. 7, pp. 1210–1212, 2002.

[19] M. A. Correa-Duarte, M. Grzelczak, V. Salgueiriño-Maceira et al., "Alignment of carbon nanotubes under low magnetic fields through attachment of magnetic nanoparticles," *Journal of Physical Chemistry B*, vol. 109, no. 41, pp. 19060–19063, 2005.

[20] Y. Dror, W. Salalha, R. L. Khalfin, Y. Cohen, A. L. Yarin, and E. Zussman, "Carbon nanotubes embedded in oriented polymer nanofibers by electrospinning," *Langmuir*, vol. 19, no. 17, pp. 7012–7020, 2003.

[21] M. Naebe, T. Lin, and X. Wang, "Carbon nanotubes reinforced electrospun polymer nanofibres," in *Nanofiber*, A. Kumar, Ed., chapter 16, pp. 209–228, InTech, Vienna, Austria, 2010.

[22] R. Haggenmueller, H. H. Gommans, A. G. Rinzler, J. E. Fischer, and K. I. Winey, "Aligned single-wall carbon nanotubes in composites by melt processing methods," *Chemical Physics Letters*, vol. 330, no. 3-4, pp. 219–225, 2000.

[23] H. Mahfuz, A. Adnan, V. K. Rangari et al., "Enhancement of strength and stiffness of Nylon 6 filaments through carbon nanotubes reinforcement," *Applied Physics Letters*, vol. 88, no. 8, Article ID 083119, 2006.

[24] V. K. Rangari, M. Y. Shaik, H. Mahfuz, and S. Jeelani, "Fabrication and characterization of high strength Nylon-6/Si_3N_4 polymer nanocomposite fibers," *Materials Science and Engineering A*, vol. 500, no. 1-2, pp. 92–97, 2009.

[25] F. Eblagon, B. Ehrle, T. Graule, and J. Kuebler, "Development of silicon nitride/silicon carbide composites for wood-cutting tools," *Journal of the European Ceramic Society*, vol. 27, no. 1, pp. 419–428, 2007.

[26] C.-A. Wang and Y. Huang, "Improved sinterability of SiC(w)/Si_3N_4 composites by whisker-oriented alignment," *Materials Science and Engineering A*, vol. 390, no. 1-2, pp. 319–325, 2005.

[27] L. A. Pérez-Maqueda, A. Duran, and J. L. Pérez-Rodríguez, "Preparation of submicron talc particles by sonication," *Applied Clay Science*, vol. 28, pp. 245–255, 2005.

[28] F. Franco, J. A. Cecila, L. A. Pérez-Maqueda, J. L. Pérez-Rodríguez, and C. S. F. Gomes, "Particle-size reduction of dickite by ultrasound treatments: effect on the structure, shape

and particle-size distribution," *Applied Clay Science*, vol. 35, no. 1-2, pp. 119–127, 2007.

[29] V. K. Rangari, T. A. Hassan, Q. Mayo, and S. Jeelani, "Size reduction of WO_3 nanoparticles by ultrasound irradiation and its applications in structural nanocomposites," *Composites Science and Technology*, vol. 69, no. 14, pp. 2293–2300, 2009.

[30] American Society for Testing Materials, "tensile strength and Young's modulus for high-modulus single-filament materials," ASTM Standard D3379-75.

[31] C. Huiqun, Z. Meifang, and L. Yaogang, "Decoration of carbon nanotubes with iron oxide," *Journal of Solid State Chemistry*, vol. 179, no. 4, pp. 1208–1213, 2006.

[32] A. G. Loera, F. Cara, M. Dumon, and J. P. Pascault, "Porous epoxy thermosets obtained by a polymerization-induced phase separation process of a degradable thermoplastic polymer," *Macromolecules*, vol. 35, no. 16, pp. 6291–6297, 2002.

[33] R. V. Kumar, Y. Koltypin, Y. S. Cohen et al., "Preparation of amorphous magnetite nanoparticles embedded in polyvinyl alcohol using ultrasound radiation," *Journal of Materials Chemistry*, vol. 10, no. 5, pp. 1125–1129, 2000.

[34] K. Chen and S. Vyazovkin, "Mechanistic differences in degradation of polystyrene and polystyrene-clay nanocomposite: thermal and thermo-oxidative degradation," *Macromolecular Chemistry and Physics*, vol. 207, no. 6, pp. 587–595, 2006.

[35] T. Liu, Y. Tong, and W.-D. Zhang, "Preparation and characterization of carbon nanotube/polyetherimide nanocomposite films," *Composites Science and Technology*, vol. 67, no. 3-4, pp. 406–412, 2007.

[36] S. Aharoni, *N-Nylons: Their Synthesis, Structure, and Properties*, John Wiley and Sons, 1998.

[37] L. Li, C. Y. Li, and C. Ni, "Polymer crystallization-driven, periodic patterning on carbon nanotubes," *Journal of the American Chemical Society*, vol. 128, no. 5, pp. 1692–1699, 2006.

[38] S. Zhang, M. L. Minus, L. Zhu, C.-P. Wong, and S. Kumar, "Polymer transcrystallinity induced by carbon nanotubes," *Polymer*, vol. 49, no. 5, pp. 1356–1364, 2008.

[39] E. T. Kopesky, G. H. McKinley, and R. E. Cohen, "Toughened poly(methyl methacrylate) nanocomposites by incorporating polyhedral oligomeric silsesquioxanes," *Polymer*, vol. 47, no. 1, pp. 299–309, 2006.